ual $\delta^{18}O$ record, which has substage 6e ~22% below peak last-interglacial values.

The Milankovitch theory in its simplest form cannot explain Termination II, as it does Termination I (*30*). However, it is still plausible that insolation forcing played a role in the timing of Termination II. As deglaciations must begin while Earth is in a glacial state, it is useful to look at factors that could trigger deglaciation during a glacial maximum. These include (i) sea ice cutting off a moisture source for the ice sheets (*31*); (ii) isostatic depression of continental crust (*32*); and (iii) high Southern Hemisphere summer insolation (*2*) through effects on the atmospheric CO_2 concentration (*33*, *34*). If ice sheets remained large during much of stage 6, the isostatic depression of the crust could have lowered the elevation of the ice sheets enough for a significant proportion of the ice sheets to have been below the equilibrium line by 145 ka, causing collapse and melting. Combined with the moisture-starving effects of extensive sea ice and the warming effects of rising CO_2 concentrations, isostatic effects could explain the early deglaciation. Further, Johnson (*35*) found a minimum in the gradient between high- and low-latitude insolation in the Northern Hemisphere at 140 ka, which would also decrease the moisture source for the ice sheets. Such a scenario would agree with models suggesting that isostatic adjustments associated with large ice sheets are a significant factor in creating the 100,000-year cycle (*32*), which is largely defined by glacial terminations.

Because there is no single clear driving mechanism for an early sea level rise during Termination II, it poses a challenge to the Milankovitch theory. The timing and cause of Termination II are particularly important because it is so closely linked to the 100,000-year cycle, of which the driving mechanism remains unclear and widely debated (*36*). With the timing of only two glacial terminations known precisely enough to test Milankovitch theory predictions, it is difficult to identify which termination is the anomaly. Corals and speleothem data from earlier terminations may help resolve the problem.

References and Notes

1. I. Winograd *et al*., *Science* **258**, 255 (1992).
2. G. Henderson, N. Slowey, *Nature* **404**, 61 (2000).
3. K. R. Ludwig *et al*., *Science* **258**, 284 (1992).
4. I. J. Winograd, J. M. Landwehr, K. R. Ludwig, T. B. Coplen, A. C. Riggs, *Quat. Res.* **48**, 141 (1997).
5. T. D. Herbert *et al*., *Science* **293**, 71 (2001).
6. C. D. Gallup, R. L. Edwards, R. G. Johnson, *Science* **263**, 796 (1994).
7. F. W. Taylor, P. Mann, *Geology* **19**, 103 (1991).
8. M. T. McCulloch, T. Esat, *Chem. Geol.* **169**, 107 (2000).
9. The OC site has two outcrops, both in roadcuts on a small road off of the main coastal highway and perpendicular to the shore. One outcrop is at the intersection with the coastal highway at an ~20-m elevation, and the other is one block uphill in a low-lying terrace at an ~30-m elevation. The lower outcrop (samples OC-4 and OC-5) contains *A. palmata* and *A. cervicornis* coral fragments, and the upper outcrop (samples OC-1 and OC-2) contains coral fragments of the same species in a loose, well-sorted carbonate sand with abundant shells and is likely part of a beach deposit. The lower outcrop is at the same elevation and approximate location as the OC site in Mesollela *et al*. (*20*) and Bender *et al*. (*37*); the upper is at the same elevation and adjacent to site AFK in (*20*) and (*37*).
10. R. L. Edwards, J. H. Chen, G. J. Wasserburg, *Earth Planet. Sci. Lett.* **81**, 175 (1987).
11. R. L. Edwards, J. H. Chen, T. L. Ku, G. J. Wasserburg, *Science* **236**, 1547 (1987).
12. R. L. Edwards, H. Cheng, M. T. Murrell, S. J. Goldstein, *Science* **276,** 782 (1997).
13. Supplementary Web material is available on *Science* Online at www.sciencemag.org/cgi/content/full/295/5553/310/DC1.
14. There could be significant error associated with the empirical model used to produce the 2000-year constraint on the accuracy of ^{230}Th ages for samples with initial $\delta^{234}U$ values within 8‰ of the modern value. Thus, it is only meant to be a rough guide to sample preservation, not a tool for correcting ages.
15. As errors vary for ^{231}Pa dates, concordancy is defined as matching within 3% of the ^{231}Pa age for samples with errors of 3% or less.
16. Other important criteria for well-preserved samples, which all of our samples meet, include (i) no evidence of inherited ^{230}Th, as indicated by a low ^{232}Th concentration; and (ii) a U concentration similar to that of modern corals of the same species.
17. The error quoted for NU-1471 and the other samples represents the 2σ analytical error. There is also systematic error associated with the error in the half-lives, which contributes $\pm$400 years for a sample of ~130 ka. Possible errors associated with diagenetic alteration are not included and are difficult to quantify.
18. D. G. Martinson *et al*., *Quat. Res.* **27**, 1 (1987).
19. The UWI-101 (Fig. 1) deposit is distinct from the downslope stage 6 material because UWI-101 does not contain head corals; its contact with the upslope stage 6 material is marked by an erosional surface that truncates a head coral (sample UWI-107).
20. K. J. Mesolella, R. K. Matthews, W. S. Broecker, D. L. Thurber, *J. Geol.* **77**, 250 (1969).
21. D. R. Muhs, K. R. Simmons, B. Steinke, *Quat. Sci. Rev.*
22. J. Imbrie *et al.*, in *Milankovitch and Climate*, A. L. Berger *et al*., Eds. (Reidel, Hingham, MA, 1984), vol. 1, pp. 269–305.
23. M. Stein *et al*., *Geochim. Cosmochim. Acta* **57**, 2541 (1993).
24. T. M. Esat, M. T. McCulloch, J. Chappell, B. Pillans, A. Omura, *Science* **283**, 197 (1999).
25. N. J. Shackleton, *Science* **289**, 1897 (2000).
26. J. R. Petit *et al*., *Nature* **399**, 429 (1999).
27. J. Chappell, N. J. Shackleton, *Nature* **324**, 137 (1986).
28. J. Chappell *et al*., *Earth Planet. Sci. Lett.* **141**, 227 (1996).
29. D. W. Lea, D. K. Pak, H. J. Spero, *Science* **289**, 1719 (2000).
30. R. G. Fairbanks, *Nature* **342**, 637 (1989).
31. H. Gildor, E. Tziperman, *Paleoceanography* **15**, 605 (2000).
32. W. R. Peltier, W. T. Hyde, *J. Atmos. Sci.* **44**, 1351 (1986).
33. J. Imbrie *et al*., *Paleoceanography* **7**, 701 (1992).
34. W. S. Broecker, G. M. Henderson, *Paleoceanography* **13**, 352 (1998).
35. R. G. Johnson, *Geology* **19**, 686 (1991).
36. D. B. Karner, R. A. Muller, *Science* **288**, 2143 (2000).
37. M. L. Bender *et al*., *Geol. Soc. Am. Bull.* **90**, 577 (1979).
38. A. L. Berger, *Quat. Res.* **9**, 139 (1978).
39. H. Cheng *et al*., *Chem. Geol.* **169**, 17 (2000).

40. C.D.G. thanks the Geology Department at the University of Maryland College Park for their support, including access to their x-ray diffraction equipment. We all thank the reviewers for helpful comments; R. Speed for key samples; R. G. Johnson and R. E. Higashi for help in the field; and L. H. Barker, chief Geologist of Barbados, and other Barbadians for assistance. Supported by NSF grants EAR-9712037, ESH-9809459, and OCE-9810724 and National Geographic grant 4887-92.

17 August 2001; accepted 21 November 2001

Iron-Silicon Alloy in Earth's Core?

Jung-Fu Lin,[1]* Dion L. Heinz,[1,2] Andrew J. Campbell,[1] James M. Devine,[1] Guoyin Shen[3]

We have investigated the phase relations in the iron-rich portion of the iron-silicon (Fe-Si) alloys at high pressures and temperatures. Our study indicates that Si alloyed with Fe can stabilize the body-centered cubic (bcc) phase up to at least 84 gigapascals (compared to ~10 gigapascals for pure Fe) and 2400 kelvin. Earth's inner core may be composed of hexagonal close-packed (hcp) Fe with up to 4 weight percent Si, but it is also conceivable that the inner core could be a mixture of a Si-rich bcc phase and a Si-poor hcp phase.

Iron is the most abundant element in Earth's core. However, the density of the outer core is about 10% lower than the density of Fe at the pressure and temperature conditions of the outer core, indicating the presence of a low atomic weight component (such as H, C, O, Si, or S) in the core (*1*). There is also evidence that the inner core may be less dense than pure Fe, and the proportion of light elements in the inner core may be as much as 3 weight % (*2–4*). The cosmochemical abundance of silicon and measured thermoelastic properties of non-silicon alloys indicate that silicon may be an important alloying element in the outer core (*5, 6*), but it was excluded as the primary alloying element in the outer core on the basis of the equation of state (EOS) of the intermediate compound

[1]Department of the Geophysical Sciences, [2]James Franck Institute, [3]Consortium for Advanced Radiation Sources, University of Chicago, Chicago, IL 60637, USA.

*To whom correspondence should be addressed. E-mail: afu@geosci.uchicago.edu

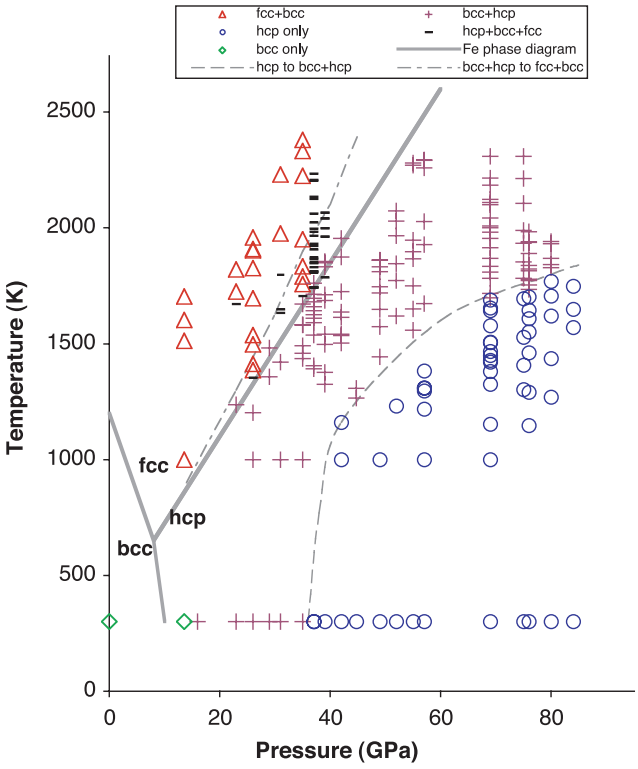

Fig. 1. Phases observed in LHDAC experiments with the starting materials of Fe(7.9 weight % Si) (*8*). The slope of the phase transformation from hcp to bcc + hcp decreases with increasing pressure. Mixed phases are commonly observed in the heating process, indicating broad regions of two phase equilibria between bcc + hcp and bcc + fcc phases. The coexistence of the bcc + hcp + fcc phases may be due to the thermal gradient, temperature fluctuation, or slight misalignment of the laser beam with respect to the x-ray beam in the LHDAC.

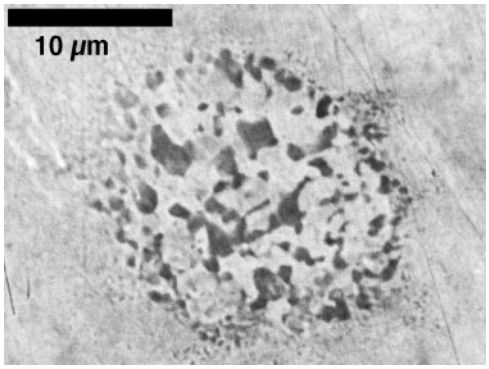

Fig. 2. Backscattered electron image of the quenched LHDAC sample from 31 GPa and 1976 K. The laser beam was ~20 μm in diameter. The average Si concentration is 11.3 (±0.3) weight % in dark areas (bcc phase) and is ~7.2 (±0.1) weight % in bright areas (fcc phase), whereas the average Si concentration remains at ~8.1 (±0.2) weight % in the surrounding unheated area.

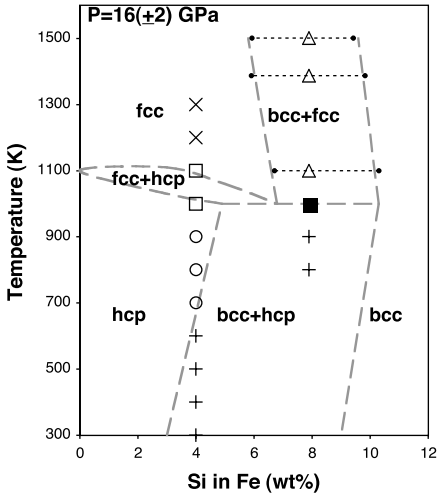

Fig. 3. Schematic *T*-X phase diagram (gray dashed lines) of iron-rich Fe-Si alloys at ~16 (±2) GPa. Crosses, bcc + hcp; ○, hcp only; □, fcc + hcp; ×, fcc only; ■, bcc + fcc + hcp; △, bcc + fcc. Tie lines indicate coexisting compositions in quenched samples that were analyzed by SEM. The experiments for Fe(4.0 weight % Si) and Fe(7.9 weight % Si) in a LVP were conducted at ~18 GPa and 14 GPa, respectively. For Fe(7.9 weight % Si) alloy, LHDAC experiments at 1387 K and 1501 K help to establish the trend of the bcc + fcc phase region.

ε-FeSi (*7*). However, studying the Fe-rich portion of the Fe-Si system is more appropriate for understanding the possible effect of Si on the EOS and the crystal structure of Fe under core conditions. The phase diagram of Fe has been extensively studied; body-centered cubic (bcc) Fe transforms to the hexagonal close-packed (hcp) phase under high pressures, and the bcc phase transforms to the face-centered cubic (fcc) phase under high temperatures (*8*). In situ x-ray diffraction studies to 161 GPa and 3000 K demonstrate that hcp-Fe has a wide stability field extending from the deep mantle to core conditions (*9*). We studied the Fe-rich portion of the Fe-Si alloys in order to understand the possible crystal structures and the phase diagram relevant to Earth's core.

The Fe(7.9 weight % Si) alloy was studied in a laser-heated diamond anvil cell (LHDAC) at pressures up to 84 GPa and temperatures up to 2400 K, and x-ray diffraction patterns were collected in situ (*10, 11*). The bcc phase transformed to the bcc + hcp phases at 16 GPa and 300 K, and the phase transformation to the hcp phase was completed at 36 GPa. When laser-heated below 16 GPa, the bcc phase transformed to a mixture of bcc + fcc phases. The hcp phase transformed to bcc + hcp phases under high temperatures and, upon further heating, bcc + hcp phases transformed to bcc + fcc phases (Fig. 1). Upon pressure quench, the sample reverted to the bcc phase. The quenched samples from a LHDAC were then analyzed with a scanning electron microprobe (SEM), and the results indicate that the starting material decomposed into two chemical compositions at high pressure and temperature (high *P-T*); the bcc phase was presumably enriched in Si, and the coexisting hcp or fcc phase was depleted in Si relative to the starting composition (Fig. 2). The partitioning of Si between bcc and hcp phases or between bcc and fcc phases indicates the presence of two-phase equilibria under high *P-T* conditions. In comparison with the phase diagram of pure Fe (*8*), it is evident that the stability field of the bcc phase can be extended to higher *P-T* conditions with the addition of Si (Fig. 1). An Fe(2.2 weight % Si) alloy was also studied in a LHDAC. This lower amount of alloying Si did not have a strong effect on the phase diagram of Fe; hcp-Fe(2.2 weight % Si) transformed entirely to the fcc phase while laser-heated at ~34 GPa to 1400 K.

To better understand the temperature-composition (*T*-X) phase diagram of Fe-Si alloys at high pressure, we also conducted in situ x-ray experiments, along with chemical analyses of the quenched samples, on Fe(4.0 weight % Si) and Fe(7.9 weight % Si) in a large-volume press (LVP) and a LHDAC (*12*) at ~16 GPa (Fig. 3) (*10*). Three regions of the two-phase equilibria are observed: bcc + hcp, bcc + fcc, and hcp + fcc. As shown, adding Si into Fe can change the phase diagram of Fe; the hcp to fcc phase transformation at lower Si contents becomes a more complicated phase transition sequence at higher Si contents (Fig. 3). The maximum solubility of Si in the fcc phase at zero pressure is only 1.9 weight % (*13*), but the effect of pressure

Table 1. Chemical analyses of the quenched Fe-Si samples. The starting material in each case was Fe(7.9 weight % Si). The measured Si contents were averaged from at least three analyses. Numbers in parentheses are SDs. These results indicate the width of the bcc + fcc or the bcc + hcp phases at the specific *P-T* conditions.

Run	*P* (GPa)	*T* (K)	bcc (Si weight %)	fcc (Si weight %)	hcp (Si weight %)	Remarks
T0250	9.4	1200 (10)	11.44 (0.13)	5.32 (0.09)		LVP; x-ray
T0258	14.1	1100 (10)	10.30 (0.08)	6.71 (0.07)		LVP; x-ray
Fe9Si#17	14.2	1501 (105)	9.42 (0.11)	5.93 (0.09)		LHDAC*
Fe9Si#18	13.9	1387 (38)	9.82 (0.12)	5.91 (0.09)		LHDAC*
Fe9Si#11	30.6	1976 (69)	11.33 (0.22)	7.19 (0.18)		LHDAC; x-ray
Fe9Si#15	42.2	1804 (17)	10.92 (0.12)		7.69 (0.10)	LHDAC*

*Fig. 1 was used for the phase identification for experiments that were conducted without x-ray.

increases the solubility of Si in the fcc phase to >6 weight % at 16 GPa (*14*) (Table 1).

Sulfur and oxygen are also considered to be two possible light elements in the core, and the properties of FeS and FeO under high *P-T* conditions have been frequently used to discuss the possibility of sulfur and oxygen in the core (*3*). Although the solubility of oxygen in Fe is low at ambient pressure, high-pressure experiments on the Fe-FeO system have shown that oxygen is soluble in Fe at high *P-T* conditions (*15*). The phase of FeS known at the highest *P-T* conditions has the hexagonal NiAs structure, which suggests that S may also form a solid solution with Fe under core conditions (*16*). As demonstrated in the Fe-Si alloy experiments reported here, a small alloying component can have a large effect on the phase diagram. Because the physical properties of the liquid often mimic the properties of the corresponding solids, it is likewise possible that adding a small alloying component to liquid Fe may also have a substantial effect on the liquid structure of Fe (*17*).

Our results show that a light element alloyed with iron can change the topology of the subsolidus phase diagram of iron under high *P-T* conditions. Adding Si into Fe stabilizes the bcc phase to much higher *P-T* conditions. However, only 2 to 4 weight % Si is not enough to change the phase diagram of Fe (Fig. 3). Therefore, if the inner core only contains 2 to 4 weight % Si, then it is likely to have the hcp structure. It is also conceivable that the inner core could be a mixture of a Si-rich bcc phase and a Si-poor hcp phase. The existence of two phases with different compositions may influence the interpretation of the observed seismic anisotropy of the inner core (*18, 19*).

References and Notes

1. F. Birch, *J. Geophys. Res.* **69**, 4377 (1964).
2. L. Stixrude, E. Wasserman, R. E. Cohen, *J. Geophys. Res.* **102**, 24729 (1997).
3. V. J. Hillgren, C. K. Gessmann, J. Li, in *Origin of the Earth and the Moon,* R. M. Canup, K. Righter, Eds. (Univ. of Arizona Press, Tucson, AZ, 2000), pp. 245–263.
4. H. K. Mao *et al*., *Science* **292**, 914 (2001).
5. A. S. Balchan, G. R. Cowan, *J. Geophys. Res.* **71**, 3577 (1966).
6. J. Zhang, F. Guyot, *Phys. Chem. Miner.* **26**, 206 (1999).
7. E. Knittle, Q. Williams, *Geophys. Res. Lett.* **22**, 445 (1995).
8. G. Shen, H. K. Mao, R. J. Hemley, T. S. Duffy, M. L. Rivers, *Geophys. Res. Lett.* **25**, 373 (1998).
9. R. Hemley, H. K. Mao, *Int. Geol. Rev.* **43**, 1 (2001).
10. For supplemental figures, see *Science* Online (www.sciencemag.org/cgi/content/full/295/5553/313/DC1).
11. The starting materials—Fe(2.2 weight % Si), Fe(4.0 weight % Si), and Fe(7.9 weight % Si) alloys in the bcc structure—were obtained from Goodfellow Corporation and W. Bassett (Cornell University) and were analyzed with an electron microprobe. The sample was ground into fine powder (grain size ~1 μm) and precompressed with a diamond anvil cell (DAC) to make a thin, flat disk. A stainless steel or rhenium gasket was pre-indented to a thickness of 25 μm, and then a hole (diameter 100 μm) was drilled in it. The diameter of the sample in a DAC was ~50 μm and the thickness was ~10 μm. A sandwiched sample configuration, using NaCl, MgO, or Ar as the thermal insulator and pressure medium, was used in this study (*20*). When NaCl or MgO was used as the thermal insulator, water contamination was eliminated by heating the DAC in a vacuum oven at 100°C for 1 hour before sealing the cell. The different pressure media were used to demonstrate that our results were independent of the pressure medium. A double-sided Nd:YLF laser heating system, operating in donut mode (TEM_{01}) or in multimode (TEM_{00} + TEM_{01}), was used to heat the sample from both sides of a DAC at the GSECARS sector of the Advanced Photon Source (APS), Argonne National Laboratory (ANL) (*20*). The laser beam diameter was ~25 μm. Alignment of the laser with the x-ray beam exploited the x-ray–induced fluorescence of the insulating pressure media. Temperatures were measured spectroradiometrically; graybody temperatures were determined by fitting the thermal radiation spectrum between 670 and 830 nm to the Planck radiation function (*20*). The laser power and the thermal radiation from the laser-heated sample were used to stabilize the temperatures in most of the experiments. The sample was laser-heated for 1 to 5 min at a target temperature, and at least three thermal radiation spectra were taken for the temperature measurement. The temperature uncertainty (1σ), averaged from multiple temperature measurements and temperatures from both sides of the sample across the laser-heated spots, was 50 to 150 K in most of the experiments. A white beam or a monochromatic beam (wavelength = 0.4246 Å) was used as the x-ray source for energy-dispersive x-ray diffraction (EDXRD) or angle-dispersive x-ray diffraction (ADXRD), respectively. The synchrotron x-ray beam was ~8 μm in diameter. The diffracted x-rays were collected by a germanium detector at a fixed angle (2θ) of ~8° in EDXRD, or by a charge-coupled device in ADXRD. All diffraction lines were identified as sample, pressure standard, pressure medium, or gasket. Pressures were calculated from the room temperature EOS of NaCl (*21, 22*) or MgO (*23*), or by the ruby fluorescence pressure scale (*24*) in the Ar medium before laser heating. No thermal pressure corrections were made to the pressures at high temperatures.
12. In situ x-ray experiments on the Fe-Si alloys were conducted in a 250-ton LVP installed at the 13-BMD beamline (GSECARS, APS). The "T-cup" multi-anvil apparatus, consisting of eight cube-shaped anvils (edge length 10 mm) made of tungsten carbide with truncated edge length of 2 mm, was used in this study (*25*). Both the starting materials [Fe(4.0 weight % Si) or Fe(7.9 weight % Si) alloy] and the pressure calibrant (Au) (*26*) were mixed with MgO powder to prevent grain growth. The sample and the pressure calibrant were packed in separate layers in the sample chamber, which was made of a mixture of amorphous boron and epoxy resin. A $W_{0.94}Re_{0.06}$-$W_{0.75}Re_{0.25}$ thermocouple was located at the center of the sample chamber for measuring the temperature. A mixture of TiC and diamond powder (1:1 by weight) was used as the internal heater, and $LaCrO_3$ semi-sintered plates were used as thermal insulation to prevent heat loss. A white beam was used as the x-ray source, and the diffracted x-rays were collimated to 100 μm × 300 μm by slits and collected by a germanium detector at a fixed angle (2θ) of ~6°. X-ray diffraction patterns were taken for phase identification while the sample was under high *P-T* conditions. Quenched samples were carefully recovered, polished, carbon-coated, and then analyzed with a SEM. No reaction between MgO and the Fe-Si alloys was observed in x-ray diffraction experiments and in a SEM.
13. O. Kubaschewski, *Iron-Binary Phase Diagrams* (Springer-Verlag, New York, 1982).
14. J. Zhang, F. Guyot, *Phys. Chem. Miner.* **26**, 419 (1999).
15. A. E. Ringwood, W. Hibberson, *Phys. Chem. Miner.* **17**, 313 (1990).
16. Y. Fei, C. T. Prewitt, H. K. Mao, C. M. Bertka, *Science* **268**, 1892 (1995).
17. C. Sanloup *et al*., *Europhys. Lett.* **52**, 151 (2000).
18. J. Tromp, *Annu. Rev. Earth Planet. Sci.* **29**, 47 (2001).
19. G. Steinle-Neumann, L. Stixrude, R. E. Cohen, O. Gulseren, *Nature* **413**, 57 (2001).
20. G. Shen, M. L. Rivers, Y. Wang, S. R. Sutton, *Rev. Sci. Instrum.* **72**, 1273 (2001).
21. F. Birch, *J. Geophys. Res.* **91**, 4949 (1986).
22. D. L. Heinz, R. Jeanloz, *Phys. Rev. B* **30**, 6045 (1984).
23. S. Speziale, C. S. Zha, T. S. Duffy, R. Hemley, H. K. Mao, *J. Geophys. Res.* **106**, 515 (2001).
24. H. K. Mao, J. Xu, P. M. Bell, *J. Geophys. Res.* **91**, 4673 (1986).
25. Y. Wang, M. Rivers, S. Sutton, P. Eng, *Rev. High Pressure Sci. Technol.* **7**, 1490 (1998).
26. D. L. Heinz, R. Jeanloz, *J. Appl. Phys.* **55**, 885 (1984).

27. The experiments were carried out at the William M. Keck High Pressure Laboratory at the GSECARS sector of the APS, ANL. We thank W. Bassett for providing Fe-Si alloys; A. Davis, I. Steele, and S. Simon for help with the chemical analyses; U. Takeyuki and S. Hongsresawat for help with LVP experiments; and M. Rivers and S. Sutton for helpful comments. Supported by NSF grant EAR-9974373 and NASA grant NAG 5-9800 (A.J.C.) to M. Humayun.

9 October 2001; accepted 21 November 2001